Multicolor Stimulated Raman Scattering Microscopy with a Rapidly Tunable Optical Parametric Oscillator

Multicolor stimulated Raman scattering microscopy with a rapidly tunable optical parametric oscillator

Lingjie Kong,† Minbiao Ji,† Gary R. Holtom, Dan Fu, Christian W. Freudiger, and X. Sunney Xie*

Department of Chemistry and Chemical Biology, Harvard University, Cambridge, Massachusetts 02138, USA
**Corresponding author: xie@chemistry.harvard.edu*

Received November 8, 2012; accepted November 30, 2012;
posted December 12, 2012 (Doc. ID 179581); published January 8, 2013

Stimulated Raman scattering (SRS) microscopy allows label-free chemical imaging based on vibrational spectroscopy. Narrowband excitation with picosecond lasers creates the highest signal levels and enables imaging speeds up to video-rate, but it sacrifices chemical specificity in samples with overlapping bands compared to broadband (multiplex) excitation. We develop a rapidly tunable picosecond optical parametric oscillator with an electro-optical tunable Lyot filter, and demonstrate multicolor SRS microscopy with synchronized line-by-line wavelength tuning to avoid spectral artifacts due to sample movement. We show sensitive imaging of three different kinds of polymer beads and live HeLa cells with moving intracellular lipid droplets. © 2013 Optical Society of America

OCIS codes: 180.4315, 180.5655, 190.4970.

Coherent Raman scattering (CRS) microscopy, a label-free, highly sensitive, chemically specific imaging technique, has recently found many applications in biomedical imaging [1–7]. Stimulated Raman scattering (SRS) microscopy [4] has emerged as an alternative to coherent anti-Stokes Raman scattering (CARS) microscopy, as it is free of spectral distortions, straightforward in contrast interpretation, and linearly dependent on analyte concentration.

Narrowband excitation with picosecond lasers for SRS microscopy is commonly used due to its spectral resolving capability and high sensitivity, and video-rate molecular imaging *in vivo* with epi-detected SRS has been demonstrated [7]. However, to distinguish M chemical components with overlapping Raman bands in complex biological samples, N ($N \geq M$) frequencies should be measured. Then, the concentration maps of individual chemical species are numerically decomposed from the N images based on multivariant analysis. Therefore, reliable multicolor SRS imaging methods are required to quantitatively resolve multiple chemical species.

In the conventional narrowband implementation of CRS microscopy for complex samples, a single Raman frequency is probed throughout an image frame, and the laser frequency is sequentially tuned frame-by-frame [8–10]. However, for live cell or tissue imaging with sample movements, such as random organelle drifting on a time scale shorter than the frame imaging time, numerical decomposition will inevitably introduce spectral artifacts due to sample motion, limiting the usefulness of frame-by-frame wavelength tuning for multicolor SRS microscopy [11].

Alternatively, femtosecond SRS [12] and multicolor SRS microscopy [13] were presented with simultaneous multichannel spectral detection, similar to multiplex-CARS microscopy [14,15]. Spectrally tailored excitation SRS microscopy [16] was demonstrated for highly specific molecular imaging, by the collective excitation of selected vibrational frequencies with a spatial light modulator based pulse-shaper. Modulation multiplexing based multiplex SRS microscopy [11] was achieved by modulating individual wavelength sub-bands within the laser bandwidth at different radio-frequencies with an acousto-optical tunable filter device. In all these techniques, the intensity information for multiple frequencies is obtained on a pixel-by-pixel basis, removing the effects of sample motion on the derived chemical species images. But in practice, their sensitivities are lower since part of the excitation power is expended on spectral bands that do not have information, which reduces the signal to noise ratio for a constant imaging time.

In this Letter, we demonstrate line-by-line wavelength tuning based narrowband SRS microscopy with an optical parametric oscillator (OPO) rapidly tuned by an electro-optical modulator, which retains the high sensitivity and reduces spectral artifacts due to sample motion.

Figure 1(a) shows the diagram of the fast tuning OPO. It is based on a commercial OPO (Levante Emerald,

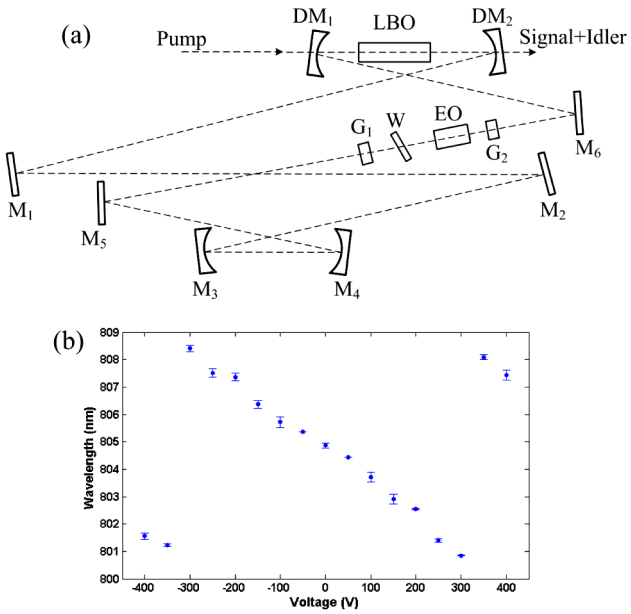

Fig. 1. (Color online) (a) Schematic of the fast tuning OPO. DM: dichroic mirror, M: mirror, G: Glan-Brewster prism, W: waveplate, EO: electro-optical crystal, LBO: lithium triborate crystal. (b) Tuning characteristic of the OPO with an electric-optical tunable Lyot filter. Dots show average values, and the error bars show the standard deviations after 100 repetitions.

APE-Berlin), which is synchronously pumped by a frequency-doubled Nd:YVO_4 mode-locked laser (76 MHz, 5 ps pulses at 532 nm, High-Q laser GmbH). The original Lyot filter is replaced by a homemade electro-optical tunable Lyot filter. Following the design shown in [17], it is made up of a static multiorder crystalline quartz waveplate (United Crystal Company), a $LiNbO_3$ based Pockel's cell (EO-AM-NR-C1, Thorlabs), and two Glan-Brewster prisms (MGLBAS5, Karl Lambrecht).

Parametric down-conversion is based on the provided temperature tuned LBO crystal (20 mm long), with type-I noncritical phase matching. It is found that even though the phase matching condition selects the intracavity polarization, the Glan–Brewster prisms are still necessary to avoid discontinuities in tuning the wavelength. The temperature of the LBO crystal and the cavity length are set to generate near-infrared signals at the desired central wavelengths, and fast wavelength tuning is accomplished by applying sequential DC voltages to the electric-optical modulator.

To achieve fast wavelength tuning, voltages on the Pockels cell are applied stepwise with homemade circuits. The tuning speed is limited by the slow slew rate of the operational amplifier (PA97DR, Cirrus Logic), which takes ~100 μs to go from −400 to +400 V. This is much longer than the timescale (~1 μs) for building-up of the steady-state operation, determined by cavity dynamics intrinsic to the OPO [17,18]. Figure 1(b) shows the wavelength tuning performance of the OPO, monitored with a fast spectrograph of 0.2 nm spectral resolution (USB 4000, Ocean Optics). Stepped voltage sweeps, increasing from −400 to 400 V monotonically with increments of 50 V and durations of 15 ms, are repeated 100 times, and the peak wavelengths are recorded. It is shown that the output wavelengths change linearly and reproducibly with the applied voltages. With a 50-λ waveplate, the achieved tuning span around 805 nm is ~7.5 nm (covering ~115 cm^{-1}), with the free spectral range determined by the sum of the waveplate birefringence and the residual static birefringence of the electro-optical crystals. For every output, the spectral bandwidth is ~0.3 nm, resulting in a spectral resolution of ~5 cm^{-1}. Unlike the results of [19], hysteresis is observed when the applied stepwise voltages are first increased and then decreased over the full voltage range (data not shown).

The SRS signal is detected using a high-frequency modulation-transfer scheme [4]. The tunable OPO signal is used as the pump beam for SRS. The 1064 nm beam is used as the Stokes beam, and is amplitude modulated at 10 MHz. The spatially and temporally overlapped pump and Stokes beams are sent through a laser scanning microscope (IX81/FV1000, Olympus) and focused onto the sample. The SRS (stimulated Raman loss) signal is detected with a homemade lock-in amplifier [7].

The FV1000 is operated in "Line Kalman" mode in which the galvos repeatedly scan each physical line for multiple times before moving to the next. We utilize the line trigger signal from the FV1000 analog interface box (FV10-ANALOG) to synchronize the driving voltages for the Pockels cell by an analog output card (PCI-6229, National Instruments) with a custom Labview program, so that each physical line is scanned sequentially N times at N preselected OPO wavelengths. Wavelength switching occurs at falling edges of the line trigger, during the retrace period of the galvos when the image data is not collected. During each frame of the two-dimensional galvo scan, N images at the corresponding Raman frequencies are constructed from the simultaneously recorded raw SRS signals (PCI-6132, with another custom Labview program) in accordance to the line trigger voltages from the FV1000. Then, the multivariant calibration based on least-squares analysis is applied to convert the raw image data into concentration maps of each chemical component [11,13].

We first evaluate the validity of spectral decomposition by imaging mixed beads coated on a cover glass, including melamine, poly(methyl methacrylate) (PMMA), and polystyrene. Their spontaneous Raman spectra are shown in Fig. 2(a) from which the desired probing wavelengths and corresponding applied voltages can be chosen. Figures 2(b)–2(d) show the SRS images (330 × 330 pixels) at 3054, 2979, 2959 cm^{-1} respectively, with a 60× objective lens (NA 1.2, water). The calibration matrix is constructed from the *in situ* imaging data of the three different beads and is used to construct the concentration image [11]. Figure 2(e) shows the RGB composite image with each color for each bead composition. It can be seen that this scheme is well suited to distinguish multiple chemical components with overlapping Raman bands.

Next, we image live HeLa cells to show the ability to minimize artifacts from organelle drifting during imaging. For cells or tissues containing primarily lipid and protein, probing at two Raman bands is sufficient to map their distribution. Here, the frequency shifts of 2838 and 2914 cm^{-1} (corresponding to pump wavelengths of 817.2 and 812.1 nm, respectively) are used. As shown in Fig. 3(a), the 2914 cm^{-1} channel is attributed to both lipid and protein, and the 2838 cm^{-1} channel is mainly attributed to the lipid. The powers at the objective focus are: 28 mW of Stokes, 81 mW at 817.2 nm, and 78 mW at 812.1 nm. The pixel dwell time for each color is 8 μs, and the wavelengths are switched every 5.184 ms (for 512 pixels per line). By picking specific regions with features corresponding to the protein and lipid, the calibration

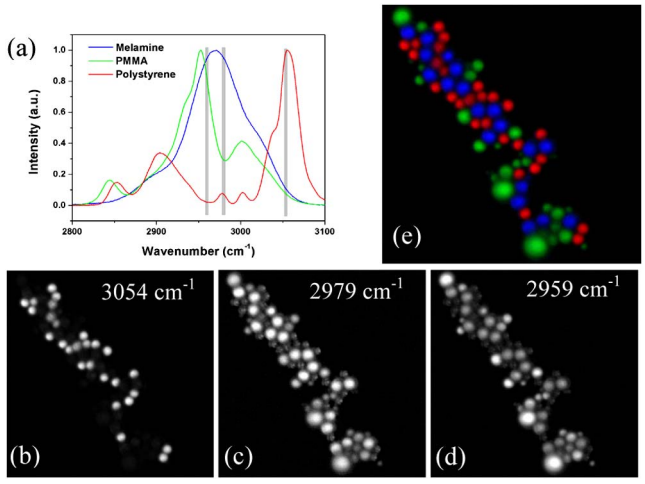

Fig. 2. (Color online) (a) Spontaneous Raman spectra of melamine, PMMA, and polystyrene beads. (b–d) Raw images taken at 3054, 2979, 2959 cm^{-1}. (e) Reconstructed SRS image (Red: 2 μm polystyrene, Green: 1–10 μm PMMA, Blue: 2.9 μm.

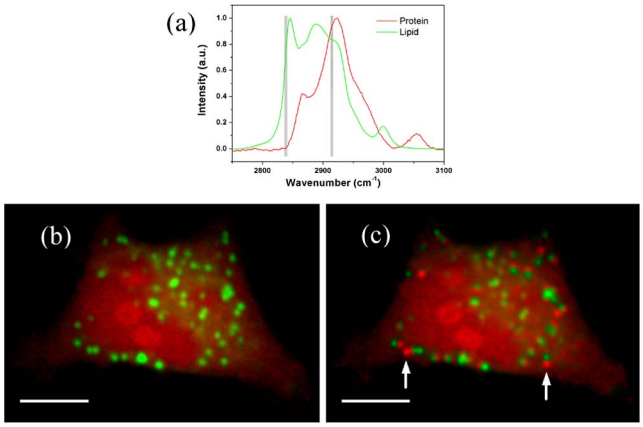

Fig. 3. (Color online) (a) Spontaneous Raman spectra of protein and lipid. (b) Reconstructed SRS image by line-by-line wavelength tuning, free of spectral artifacts due to lipid droplet driftings. (c) Reconstructed SRS image by frame-by-frame wavelength tuning. Two arrows point to artifacts due to lipid droplet driftings. Red: protein, green: lipid. Both images are 460×318 pixels. The scale bar is 10 μm (60× water objective lens used).

matrix is created [11]. Figure 3(b) shows the retrieved image of the HeLa cell, which shows the distribution of protein and lipid. Lipid droplets are shown in green, and protein is shown in red throughout the cytoplasm and nucleus. In comparison, the retrieved image from sequential frame-by-frame wavelength tuning is shown in Fig. 3(c). After decomposition, the moving lipid droplets introduce artifacts as protein signals, such as the red droplets marked with arrows, which is obviously due to lipid droplet motion when compared with Fig. 3(b).

In conclusion, we develop a rapidly tunable OPO with an electro-optical tunable Lyot filter for multicolor SRS microscopy. With repeated line scanning, all the necessary spectral information for each image line (512 pixels) is recorded in about 5 ms per spectral component. Compared to frame-by-frame sequential wavelength tuning, this minimizes spectral artifacts due to sample motions. This system can either be used for high-speed hyperspectral imaging to obtain the spectroscopic information of the sample [9,10], or for multispectral imaging with rapid random access to any Raman shift within the tuning span. Combining random-access line-by-line tuning with video-rate multicolor imaging [10] would provide the ultimate solution to maximize sensitivity and imaging speed while avoiding spectral artifacts and blur [7] due to motions.

We thank Fa-ke Lu and Wenlong Yang for help on preparing samples and discussions. This work was supported by the National Institute of Health's T-R01 (1R01EB010244-01) awarded to X. Sunney Xie.

†Authors contributed equally to this work.

References

1. A. Zumbusch, G. R. Holtom, and X. S. Xie, Phys. Rev. Lett. **82**, 4142 (1999).
2. J. X. Cheng, A. Volkmer, L. D. Book, and X. S. Xie, J. Phys. Chem. B **105**, 1277 (2001).
3. C. L. Evans and X. S. Xie, Annu. Rev. Phys. Chem. **1**, 883 (2008).
4. C. W. Freudiger, W. Min, B. G. Saar, S. Lu, G. R. Holtom, C. He, J. C. Tsai, J. X. Kang, and X. S. Xie, Science **322**, 1857 (2008).
5. Y. Ozeki, F. Dake, S. I. Kajiyama, K. Fukui, and K. Itoh, Opt. Express **17**, 3651 (2009).
6. P. Nandakumar, A. Kovalev, and A. Volkmer, New J. Phys. **11**, 033026 (2009).
7. B. G. Saar, C. W. Freudiger, J. Reichman, C. M. Stanley, G. R. Holtom, and X. S. Xie, Science **330**, 1368 (2010).
8. C.-Y. Lin, J. L. Suhalim, C. L. Nien, M. D. Miljkovic, M. Diem, J. V. Jester, and E. O. Potma, J. Biomed. Opt. **16**, 021104 (2011).
9. Y. Ozeki, W. Umemura, K. Sumimura, N. Nishizawa, K. Fukui, and K. Itoh, Opt. Lett. **37**, 431 (2012).
10. Y. Ozeki, W. Umemura, Y. Otsuka, S. Satoh, H. Hashimoto, K. Sumimura, N. Nishizawa, K. Fukui, and K. Itoh, Nat. Photonics **6**, 845 (2012).
11. D. Fu, F.-K. Lu, X. Zhang, C. Freudiger, D. R. Pernik, G. Holtom, and X. S. Xie, J. Am. Chem. Soc. **134**, 3623 (2012).
12. E. Ploetz, S. Laimgruber, S. Berner, W. Zinth, and P. Gilch, Appl. Phys. B **87**, 389 (2007).
13. F.-K. Lu, M. Ji, D. Fu, X. Ni, C. W. Freudiger, G. Holtom, and X. S. Xie, Mol. Phys. **110**, 1927 (2012).
14. J. X. Cheng, A. Volkmer, L. D. Book, and X. S. Xie, J. Phys. Chem. B **106**, 8493 (2002).
15. G. W. H. Wurpel, J. M. Schins, and M. Muller, Opt. Lett. **27**, 1093 (2002).
16. C. W. Freudiger, W. Min, G. R. Holtom, B. Xu, M. Dantus, and X. S. Xie, Nat. Photonics **5**, 103 (2011).
17. B. G. Saar, G. R. Holtom, C. W. Freudiger, C. Ackermann, W. Hill, and X. S. Xie, Opt. Express **17**, 12532 (2009).
18. A. Godard and E. Rosencher, IEEE J. Quantum Electron. **40**, 784 (2004).
19. M. D. Ewbank, M. J. Rosker, and G. L. Bennett, J. Opt. Soc. Am. B **14**, 666 (1997).